Development of single grain OSL dating of ceramic materials: spatially resolved measurement of absorbed dose

I.K.Bailiff

Luminescence Dating and Dosimetry Laboratory, Department of Archaeology, Dawson Building, University of Durham, South Road, Durham DH1 3LE, UK

The feasibility of using an OSL scanning technique to determine the cumulative absorbed dose for single inclusions in sliced brick samples is explored in this paper. The OSL scanner was configured to provide optical stimulation using laser sources with either blue/green or near-IR wavelengths. A regenerative OSL procedure was successfully applied to determine the palaeodose for single grains of quartz in the surface of the ceramic slices ranging in diameter from ~60 μm to ~750 μm. The results obtained compare well with calculated values of palaeodose obtained by scaling the measured values of palaeodose obtained using a single aliquot regenerative procedure with disaggregated quartz inclusions extracted from the same brick and prepared using the conventional inclusion technique.

Keywords: luminescence dating, single grain, spatially-resolved

*Corresponding author:

e-mail: Ian.Bailiff@durham.ac.uk, fax: +44-191-334-1101; phone: +44-191-334-1124

1. Introduction

The feasibility of using an OSL scanning technique to determine the cumulative absorbed dose for single inclusions embedded in sliced ceramic samples has been demonstrated in previous work (Bailiff and Mikhailik, 2003). The application of this approach to dating measurements with archaeological ceramic samples on a grain-by-grain basis is of interest in cases where, for example, only a small fragment is available or where the distribution of lithogenic radionuclides in the sample matrix is heterogeneous. The general problem of confinement of the measured luminescence to a very small proportion of grains has been long recognised (Huntley and Kirkey, 1985) and this undermines a basic assumption of the method if the radiation field due to radionuclides of lithogenic origin within the sample is strongly non-isotropic. Elements of the methodological approach developed by Aitken and Wintle (1977; also Aitken, 1985, in respect of the measurement of *a* value) for dating slices of calcite and flint are relevant, although not directly applicable to single grains in ceramic slices. The aim of the experiment was to investigate whether bright grains were present in brick samples and, if so, to apply a regenerative procedure using the OSL scanner to determine the palaeodose for individual grains. The slices of ceramic examined were cut from bricks that previously had been dated using disaggregated HF-etched quartz inclusions for which determinations of the palaeodose were available for comparison.

2. Experimental

2.1 Samples

Slices were extracted from two brick cores (refs 294-17 and 304) that had been obtained as part of an on-going programme of dating of a group of English late medieval buildings. These samples were selected because of their bright OSL signals and the high experimental precision obtained in the measurement of the palaeodose. Using a diamond wafering blade,

slices of 1 mm thickness were cut from brick rods of ~15 mm length (~ 10 mm x 12 mm in cross-section) that had been encapsulated in a cold-setting resin. After removal of the resin by immersion in a solvent, the slices were fastened to machined stainless steel plates using a cyanoacrylate glue. All preparation was performed under subdued red lighting conditions and exposure to (red) light was kept to a minimum to avoid optical bleaching of the exposed surfaces. No further polishing or treatment of the surface was undertaken.

2.2 Instrumentation

Spatially resolved OSL measurements with the slices were performed using an OSL scanner that is based on the system described previously (Bailiff and Mikhailik, 2003). The distribution of OSL is obtained within an area of 10 mm x 10 mm based on data from 1600 measurement points when using a step size of 250 μm. The optical stimulation beam is directed onto the sample surface at a constant angle (~ 45º) after passing through an electronically controlled shutter, selected optical filters and a beam-focusing lens. In these experiments the sample was moved under the path of the beam in a stepwise manner; after each incremental move, the shutter was opened for a selected stimulation period (e.g., 200 ms) during which the sample was exposed to the laser beam and the OSL recorded.

Three types of optical stimulation source were used: a constant wave (CW) source provided by the output of an Ar-ion laser (Reliant 250D, Laser Physics) operated in multi-line mode (488/514 nm lines dominant); a CW 850 nm laser diode (Laser 2000) and a pulsed diode-pumped solid-state laser (YAG:Nd; Laser 2000) that was frequency doubled to provide emission at 532 nm. The laser beam spot diameter at the sample position was adjusted to ~250 μm using the knife-edge technique to measure the intensity profile. The beam intensity and position were monitored using a silicon photodiode with a pin-hole aperture placed in the

sample position, and the power was adjusted either by regulation of the laser power or by optical attenuation of the beam.

The luminescence was detected by an EMI 9635QA PMT after passing through a Schott U-340 filter (6 mm), the signal from the PMT anode was passed via a fast charge-sensitive preamplifier and discriminator to a multi-channel scalar (MCS), as described previously (Bailiff and Mikhailik, 2003). When using the pulsed laser stimulation source, a time-window discriminator (Redut Ltd) and dual-channel MCS (FAST Comtec GmbH) were substituted for the corresponding elements in the above configuration to distinguish prompt (< 1 μs) and delayed (>1 μs) recombination luminescence detected following the arrival of each laser pulse (Bailiff and Mikhailik, 2003). OSL measurements for disaggregated quartz grains were performed using a Risø DA 12 semi-automated reader (Risø National Laboratory) under optical stimulation with blue LEDs.

Absorbed doses were administered to grains located on stainless steel discs using the standard $^{90}Sr/^{90}Y$ irradiator mounted on the reader, the dose-rate from which had been calibrated against a secondary photon source (^{60}Co; Göksu et al., 1995) at the GSF Secondary Standards Dosimetry Laboratory (SSDL). Slices were irradiated using a beta irradiator (Bailiff, 1980), containing a similar type of $^{90}Sr/^{90}Y$ beta source, the spatially-resolved dose-rate from which was calibrated with quartz grains that had been irradiated with a known dose (1 Gy) by a ^{60}Co source at the GSF SSDL, as discussed further below.

2.3 Procedures for the measurement of absorbed dose

The absorbed dose to both disaggregated grains and grains within the surface of slices was determined following an OSL single aliquot regenerative procedure (Bailiff and Holland,

2000) that is similar to that described by Murray and Wintle (2000) and which included the monitoring and correction of sensitivity change due to sensitization effects. Increases in OSL sensitivity are generally slight for samples of this age and type since the palaeodose (typically1-2 Gy) and the temperatures, T_P, used in the preheat treatment are sufficiently low to avoid the onset of significant sensitization. Unless stated otherwise, the beta doses administered ranged from 0.8 to 1.2 of the estimated palaeodose, P. The preheating procedure applied to slices (holding the sample at 220˚C for 10s) was selected after examination of the position of the palaeodose plateau (P vs T_P) obtained with disaggregated quartz grains from the same sample and taking into account the effects of thermal lag.

2.4 Spatially –resolved calibration of beta source dose-rate

The beta source dose-rate to quartz grains in the sub-surface of 1 mm-thick slices of ceramic was measured using single grains of quartz irradiated with a dose of 1 Gy at the GSF SSDL. The latter were distributed in an array of shallow holes cut into the surface of a slice of ceramic tile prepared for use in calibration. A regenerative procedure using scanning measurements was applied to obtain the absorbed dose (units of time) at each location where a sufficiently bright grain was detected. Using these data, the measured dose-rate to 90-150 μm diameter single grains located in the central region of the sub-surface of the 1 mm-thick ceramic slice was 1.02±0.07 Gy min^{-1}. The relative variation of the measured source dose-rate with radial distance in the sub-surface plane is shown in Fig. 1 for measurement points within one half of the irradiated area. It compares well with that predicted by Monte Carlo simulations performed for this particular irradiation geometry using the MCNP code (Forster et al., 2004), although the source dose rate in one quadrant of the irradiated area showed a stronger reduction with radial distance and this is to be investigated in more detail. Monte Carlo simulations of beta particle transport were also performed to obtain the dose-depth

profile in a 1 mm-thick ceramic slice for the specific irradiation conditions. The relative spatial variation in source dose-rate is also similar to that observed experimentally by Spooner and Allsop (2000) who used the same type of silver plaque source.

3. Results

3.1 Single grains in brick slices

The OSL data were collected in two consecutive scans to optimise the signal-to-noise ratio. Regions of bright emission were identified by producing contour plots of the recorded photon counts (obtained using either 514 nm or 850 nm radiation). Fig. 2 shows an example of an OSL contour map obtained with sample 294-17-S4, and the corresponding photographic image of the slice is shown in Fig. 3. Visual inspection and correlation of the two images at macroscopic and microscopic levels was performed to identify the sources of luminescence evident in the OSL map. For example, a grain of ~500 μm diameter highlighted in Fig. 3 can be correlated with a region of relatively intense OSL emission in the contour plot (Fig. 2).

Providing the first OSL scan (natural dose) indicated sufficiently bright emission, a regenerative procedure was applied to determine the palaeodose for the one or more grains located within each emitting area. Between each stage of the regenerative procedure the slices were exposed to white light from an unfiltered tungsten-halogen lamp for at least 25 mins to ensure trapped charge depletion. Following completion of the OSL regenerative procedure using 488/514 nm stimulation, each slice was scanned using either 850 nm (CW) or 532 nm (pulsed) laser radiation following administration of a beta dose to identify the location of feldspar emissions; for the two samples discussed here the majority of bright grains detected were attributed to quartz.

The areas delineated by analysis of the first OSL scan as showing the brightest emission were used as the basis for signal integration in all subsequent scans of the slice. These data were plotted as growth characteristics to determine the palaeodose for each area. As expected from the measurements with disaggregated grains, the growth characteristics showed a linear dependence of OSL signal with dose within experimental error of ±5% (for brevity, not shown). The calculation of P was performed initially in units of (irradiation) time and then converted to absorbed dose in quartz (mGy) using the spatially resolved calibration of the beta source. Table 1 presents values of palaeodose, P_{SG}, obtained for the bright areas in each slice (denoted surface grain) that were subsequently identified as single grains by visual examination, together with their estimated grain size. The average values of palaeodose, P_i, obtained with disaggregated quartz grains extracted from each sample are also shown in the table. The term surface grain is used below to refer to both abraded and unabraded grains.

3.2 Comparison of palaeodose - HF etched quartz and single grains in slices

A comparison of the values of palaeodose obtained using the two experimental procedures was performed by scaling the value of P_i, measured with HF etched grains, to obtain the predicted values of effective absorbed dose for surface grains of specified size in the surface of a slice, ${}_{cal}P_{SG}$. The scaling factor, S_C, was calculated as the ratio of the total dose rate for the surface grain, $\dot{D}_{SG}$, to that for disaggregated HF etched grains, $\dot{D}_i$,

$$ {}_{cal}P_{SG} = P_i \cdot S_C = P_i \cdot (\dot{D}_{SG} / \dot{D}_i) \qquad (1) $$

$\dot{D}_i$ was obtained by summing the β, γ and cosmic dose-rate ($\dot{D}$) components for the quartz inclusion technique (Aitken, 1985), including lumped coefficients b and g to account for attenuation effects and irradiation geometry:

$$ \dot{D}_i = b\,\dot{D}_\beta + g\,\dot{D}_\gamma + \dot{D}_c \qquad (2) $$

The calculation of $\dot{D}_{SG}$ requires an estimation of the relative contributions of α, β, γ and cosmic radiation to the volume of the grain remaining in the slice. The contribution of alpha radiation to the total dose-rate varies according to the size of the grain and the extent to which it has been abraded. Examination of the slice surface indicated that the smaller grains were likely to have been either mechanically removed from the surface or remain intact with slight abrasion, and that the larger grains (e.g., >150 μm dia.) were usually abraded, although there were some instances where the blade cut through cavities above grains leaving them intact. Taking these considerations into account, the dose-rate to the volume corresponding to the surviving portion of grain, when located in the undisturbed matrix, was calculated on the basis of the volumes penetrated by each radiation type, as indicated in Fig. 4.

If the grain is exposed by cutting but is not abraded,

$$\dot{D}_{SG} = (b\,\dot{D}_{\beta} + g\,\dot{D}_{\gamma} + \dot{D}_{c}) + (V_G - V^i) \cdot (a'\,\dot{D}_{\alpha}) / V_G, \quad (3)$$

where the dose-rates $\dot{D}$ and the coefficients b and g are defined in Eq. (2), a′ represents a lumped coefficient to account for alpha efficiency and irradiation geometry, V_G and V^i, are the volumes of the whole grain and the inner grain volume of radius ($R - \alpha_R$) not penetrated by alpha irradiation respectively.

If the grain is abraded, the dose rate is given by the following expression:

$$\dot{D}_{SG} = (b'\,\dot{D}_{\beta} + g\,\dot{D}_{\gamma} + \dot{D}_{c}) + (V_{cap} - V^i_{cap}) \cdot (a'\,\dot{D}_{\alpha}) / V_{cap}, \quad (4)$$

where the volumes V_{cap} and V^i_{cap} within an abraded grain are those below the plane of cutting, as indicated in Fig. 4, and where the lumped coefficient b for the abraded grain is denoted b'. The formulae for the volumes V_{cap} and V^i_{cap} can be expressed in terms of the grain radius R, the parameter h and the alpha range α_R, as discussed in the caption to Fig. 4.

The following assumptions were made when evaluating Eqs. (3) and (4): i) the alpha particle effectiveness and range were 0.10±0.03 and 20 μm respectively, and the irradiation geometry

was 2π; ii) the grains were spherical; iii) the OSL sensitivity and transparency of the grains were assumed to be uniform; iv) the distribution of dose within single grains due to γ and cosmic radiation was uniform. Also, when evaluating Eq. (4), it was assumed that larger grains (>200 μm dia.) were abraded during cutting to a depth corresponding to half their radius. The predicted change in the total dose-rate, D_{SG}, with the degree of abrasion (i.e., h) calculated using Eqn 4 and making the above assumptions is shown in Fig. 5 for unetched grains of diameter 100 μm and 500 μm.

The dose-rates $\dot{D}$ used in the calculation are based on measured rather than hypothetical data and the values of attenuation factors for spherical grains irradiated by beta particles emitted by lithogenic radionuclides in the surrounding medium were taken from Brennan (2003). In the case of the abraded grains, the value of the lumped coefficient b′ differs from that for an unabraded grain because the beta dose within the unabraded grain generally decreases with depth from the surface of the grain due to the effects of attenuation. The distribution of beta dose consequently changes in an abraded grain (except where a spherical grain cut in half), the extent of which depends on the degree of abrasion. Estimates of b′ were obtained using a simple spherical grain model that accounts for the changes in the proportions of volumes within the grain (as concentric spherical shells) with the degree of abrasion and the absorbed dose profile within the grain (simulated using MCNP for a ^{40}K beta decay energy spectrum). These calculations indicate that the value of b′ is generally higher than that of b due to the increased weighting by the outer layers of the grain that have received a higher absorbed dose relative to volumes closer to the centre of the grain. However, for the grain size ranges relevant to the samples discussed here, the increase is slight (~5%), and this has been taken into account when performing an analysis of uncertainty in $\dot{D}_{SG}$, as discussed further below.

Finally, the values of ${}_{cal}P_{SG}$ (= $S_C \cdot P_i$) calculated for each sample are shown in Figs 6a,b (open circles) for a range of grain diameters in the surface of the slice and these are to be compared

with the experimental values P_{SG} for the surface grains in the slice (open triangles). The experimental value of P_i for HF etched quartz, from which the calculated values ${}_{cal}P_{SG}$ were derived by scaling, is also shown (filled square). To obtain a measure of the effect of uncertainty in the extent of abrasion of the larger grains, a Monte Carlo simulation (using the software program Crystal Ball, Decisioneering Inc.) of the calculation of ${}_{cal}P_{SG}$ was performed in which the depth of the surviving portion of grain, h, was allowed to vary within a range of a quarter of the grain diameter, and the distribution obtained was used to define the uncertainty in the values shown in Figs. 6a,b. As indicated in Fig. 5, the sensitivity of the total dose-rate, $\dot{D}_i$, to variation in h is not particularly strong (according to this approximation). Since the beta source was calibrated for sub-surface grains (90-150 μm dia.), an additional adjustment was made to ${}_{cal}P_{SG}$ for grains larger than 200 μm to account for the reduction for the source dose-rate with depth in the slice.

4. Discussion

The finding of a relatively small number of bright grains (Fig. 2) was generally consistent with scans obtained with other slices tested from the same and similar samples. It was surprising to find that the value of P obtained with disaggregated HF etched quartz grains extracted from sample 294-17 was measured with relatively high precision since the fabric has a generally heterogeneous composition (Fig. 3). This is relevant to the investigation of samples that exhibit significant scatter in the value of palaeodose and where the cause could be related to the sporadic distribution of a small number of bright grains in a fabric arising from a strongly heterogeneous beta radiation field or, on the other hand, an undetected factor associated with the properties of the quartz inclusions that affects the determination of P.

The greater spatial extent of the OSL associated with a single grain compared with its physical size (e.g., the large grain within slice 294-17 circled in Fig. 3) is a consequence of beam size and localised scattering of laser light at the slice surface. The beam diameter (FWHM ~250 μm and FWQM ~500 μm) was adjusted to be equivalent to the step size to obtain continuity of optical stimulation and also tolerance to small differences in sample positioning (i.e., 50 μm). In this respect the scanner has been optimised for the measurement of a relatively small number of bright grains in an opaque matrix and the aim has not been to perform imaging, as with a CCD system (e.g. Spooner, 2000; Habermann et al., 2000; Greilich et al., 2002). The extent of optical bleaching of grains located beyond the stimulation area due to scattered light was also investigated in previous tests. Measurements with grains located in areas stimulated towards the start and finish of a scan indicated that the level of bleaching during a scan (typically lasting 50 mins) due to scattered laser light was less than 10%. Providing the series of scanning measurements applied to a slice remains unaltered throughout the regenerative sequence, this level of bleaching is not expected to give rise to systematic differences in the value of absorbed dose due to the position of an emitting grain in the scan sequence.

Turning to the values of P_{SG} (Figs 6a,b and Table 1) obtained for single grains in the two slices, reasonably consistent values were obtained for grains judged to be of similar size. For grains of nominal diameter 200 and 100 μm the average values of P for samples 294-17 and 304 were 1560±70 mGy (s.d. 3) and 1910±55 mGy (s.d. 4) respectively. Despite the potential for variability in this type of experiment, the relative error is comparable to that obtained with HF etched disaggregated grains. The trend in the reduction of the experimental values of palaeodose with increasing grain size is also consistent with expectation. The level of agreement achieved between the average experimental values and the corresponding

calculated values is reasonable in view of the series of assumptions and approximations made. The differences in the central values of the experimental data (1560±70 mGy and 1910±55 mGy) and the corresponding predicted values (1820±50 mGy and 1780±85 mGy) for grains located in the sliced samples represent an underestimate of 15% and an overestimate of 9% for samples 294-17 and 304 respectively. Given the approximations discussed above, this level of agreement is encouraging.

5. Conclusions

Although, from a dosimetry perspective, the experimental approach required to measure absorbed dose for single grains in slices is inevitably more complex than the quartz inclusion method, it has the potential to provide information concerning absorbed dose that is not available by performing measurements with disaggregated grains. The results of the experiments described in this paper suggest that reliable determinations of palaeodose can be obtained with single quartz grains, judged in this case against the conventional quartz inclusion technique. In particular, it provides a means of investigating the issue of a non-isotropic radiation field in the sample matrix and, ultimately, the possibility of dating single grains *in situ* if the experimental difficulties of microdosimetry of the immediate grain environment can be overcome, an issue that harks back to earlier research (e.g., Miallier et al., 1985).

Acknowledgements

I am grateful to Mr. S. Grainger and for technical assistance, to Dr H. A. Slim for performing the Monte Carlo simulations of radiation transport in slices using the MCNP code that forms part of a research project (#F/00128/AA) supported by the Leverhulme Trust. I also thank

Rachel Wood for making contributions to the testing of the scanner as part of a Nuffield Undergraduate Research Bursary project.

References

Aitken, M.J., 1985. Thermoluminescence Dating. Academic Press, London.

Aitken, M.J., Wintle, A.G., 1977. Thermoluminescence dating of calcite and burnt flint: the age relation for slices. Archaeometry 19, 100-105.

Bailiff, I.K., (1980) A beta irradiator for use in TL dating at the Durham TL Dating Laboratory. Nucl. Instrum. and Methods, 175, 224 -226.

Bailiff, I.K., Holland, N., 2000. Dating bricks of the last two millennia from Newcastle upon Tyne: a preliminary study. Radiat. Meas. 32, 615-619.

Bailiff, I.K., Mikhailik, V.B, 2003. Spatially resolved measurement of optically stimulated luminescence and time-resolved luminescence. Radiat. Meas. 37, 151-159.

Brennan, B.J., 2003. Beta doses to spherical grains. Radiat. Meas. 37, 299-303.

Forster, R.A., Cox, L.J., Barrett, R.F., Booth, T.E., Breimeister, J.F., Brown, F.B., Bull, J.S., Geisler, G.C., Goorley, J.T., Mosteller, R.D., Post, S.E., Prael, R.E., Selcow, E.C., Sood, A., 2004. MCNP^{TM} version 5. Nucl. Instrum. and Methods B 213, 82-86.

Göksu, H.Y., Bailiff, I.K., Boetter-Jensen, L., Hütt, G., Stoneham, D., 1995. Inter-laboratory beta source calibration using TL and OSL with natural quartz. Radiat. Meas. 24, 479-484.

Greilich, S., Glasmacher, U.A., Wagner, G.A., 2002. Spatially resolved detection of luminescence – a unique tool for archaeochronometry. Naturwissenschaften 89, 371-375.

Habermann, J., Schilles, T., Kalchgruber, R., Wagner, G.A., 2000. Steps towards surface dating using luminescence. Radiat. Meas. 32, 847-851.

Huntley, D.J., Kirkey, J.J., 1985. The use of an image intensifier to study the TL intensity variability of individual grains. Ancient TL 3, 1-4.

Miallier, D., Fain, J., Sanzelle, S., 1985. Single-quartz-grain thermoluminescence dating: An approach for complex materials. Nucl. Tracks and Radiat. Meas. 10, 163-168.

Murray, A.S., Wintle, A.G., 2000. Luminescence dating of quartz using an improved single-aliquot regenerative–dose protocol. Radiat. Meas. 32, 57-73.

Spooner, N.A., 2000. A photon-counting imaging system (PCIS) for luminescence applications. Radiat. Meas. 32, 513-521.

Spooner, N.A., Allsop, A. (2000) The spatial variation of dose-rate from $^{90}Sr/^{90}Y$ beta sources used in luminescence dating. Radiat. Meas. 32, 49-56.

Table 1. Summary of values of palaeodose obtained with HF etched grains and single grains in slices from samples 294-17-S4 and 304-S2.

	294-17-S4		304-S2	
	Grain size (μm)	P (mGy)	Grain size (μm)	P (mGy)
HF etched	125±25	1670±35	125±25	1514±16
Grains in slice				
Surface Grain #1	200±50	1620±80	60±20	2190±110
#2	200±50	1570±80	100±30	1950±100
#3	200±50	1480±75	100±30	1870±95
#4	750±150	1130±55	100±30	2005±100
#5			200±50	1765±90

Figure captions

Fig. 1. Variation in beta source dose-rate with distance from the central axis. The open circles represent experimental determinations of source dose-rate to the sub-surface of a 1 mm-thick ceramic slice using 90-150 μm quartz grains, as discussed in the main text. The filled triangles represent the calculated values of absorbed dose based on Monte Carlo simulations of electron transport in the ceramic slice. Each set of data is normalised to the initial value of dose.

Fig. 2. Contour plot of OSL distribution for slice 294-17-S4, measured using blue/green stimulation wavelengths (488/514 nm); the dimensions of both axes are μm.

Fig. 3. Photographic image of slice 294-17-S4 bonded to its metal positioning plate. The width of the slice is 13 mm. The area contained in the white circle is a grain of ~500 μm diameter at the surface and which was located just below the cutting blade and consequently not abraded. The darkest areas are fissures in the fabric.

Fig. 4. Geometric cross section of a spherical grain, of volume V_G, that identifies the radius (R), the depth of penetration of alpha radiation (α_R) and the depth, h, of the surviving part of the grain in the ceramic slice after cutting as indicated by the dotted line. The difference between the volumes V_{cap} and V^i_{cap} in the surviving part of the grain below the cutting plane represents the portion of the grain that would have been penetrated by α radiation, whereas both volumes are penetrated by β, γ and cosmic radiation.

Fig. 5. Variation in total dose-rate $\dot{D}_{SG}$ with h (see Fig. 4) for unetched grains calculated using the approximations described in the main text, for grain diameters of 100 μm (open circles) and 500 μm (filled circles). The values of $\dot{D}_{SG}$ were normalised to the total dose-rate, $\dot{D}_i$, for HF etched grains of diameter 90-150 μm.

Fig. 6. Values of absorbed dose (palaeodose) vs mean grain diameters for slices a) 294-17-S4 and b) 304-1-S2. The experimental values, P_i and P_{SG}, are shown as open triangles and as a filled square for single grains in the slice and 90-150 mm disaggregated HF etched grains respectively. The uncertainties in the single grain diameters are estimates. The open circles represent the predicted values of absorbed dose, calculated using the approach discussed in

the main text, ${}_{cal}P_{SG}$, to single grains of the size indicated that were calculated using the approach discussed in the main text.

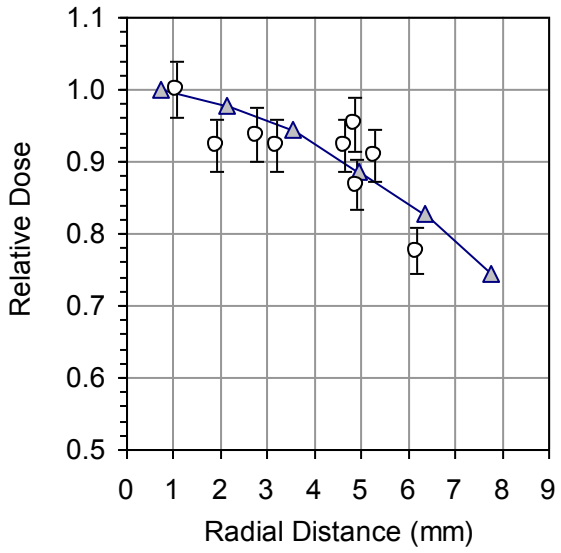
Relative Dose
1.1
1.0
0.9
0.8
0.7
0.6
0.5
0
1
2
3
4
5
6
7
8
9
Radial Distance (mm)

Fig. 1

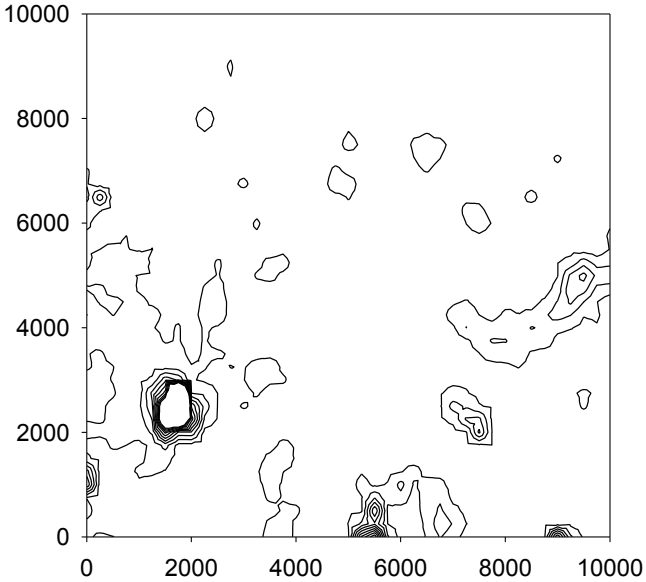

Fig. 2

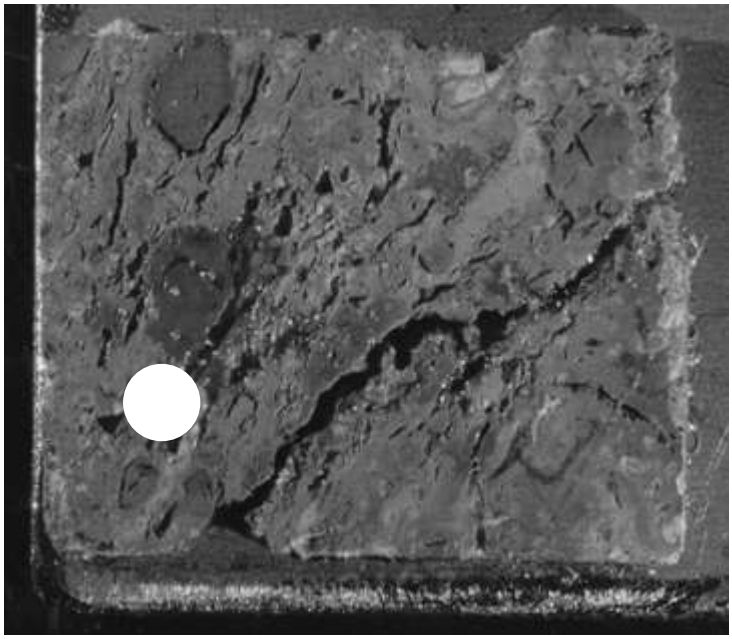

Fig. 3

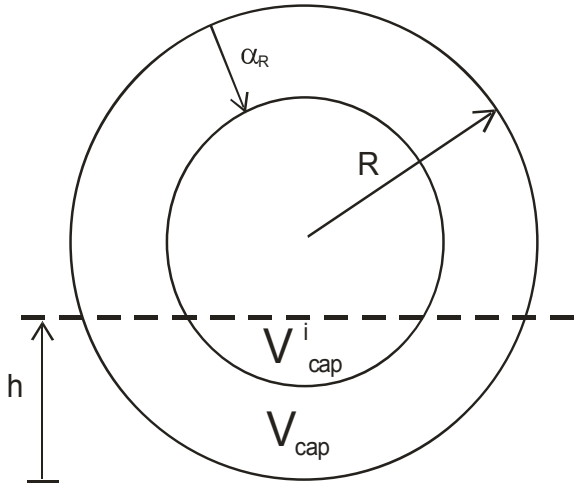

Fig. 4

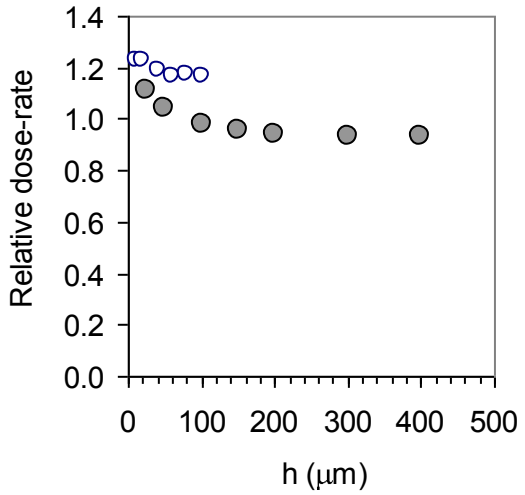
1.4
1.2
1.0
0.8
0.6
0.4
0.2
0.0
Relative dose-rate
0
100
200
300
400
500
h (μm)

Fig. 5

a)

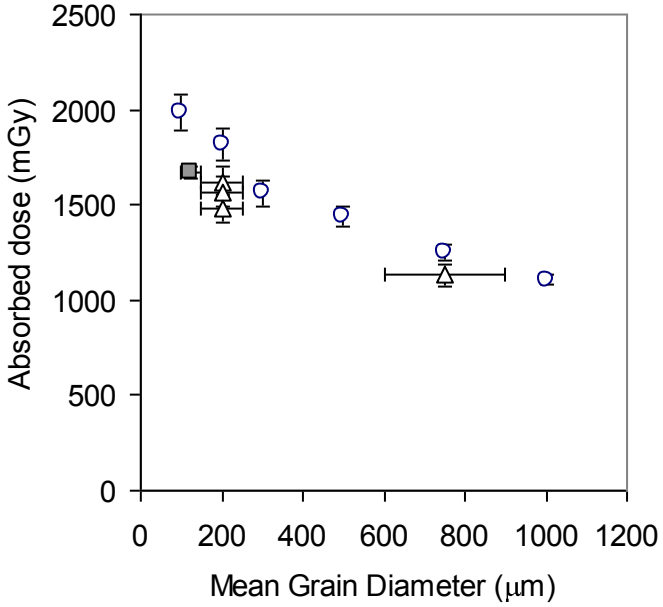
2500
2000
1500
1000
500
0
Absorbed dose (mGy)
0
200
400
600
800
1000
1200
Mean Grain Diameter (μm)

b)

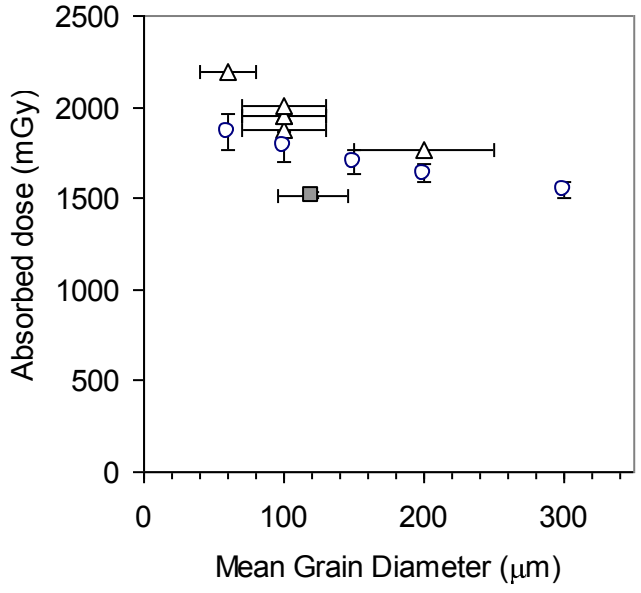
2500
2000
1500
1000
500
0
Absorbed dose (mGy)
0
100
200
300
Mean Grain Diameter (μm)

Fig. 6